SCIENTIFIC REPORTS
nature research

OPEN

Excitation of Faraday-like body waves in vibrated living earthworms

Ivan S. Maksymov[1] & Andrey Pototsky[2]

Biological cells and many living organisms are mostly made of liquids and therefore, by analogy with liquid drops, they should exhibit a range of fundamental nonlinear phenomena such as the onset of standing surface waves. Here, we test four common species of earthworm to demonstrate that vertical vibration of living worms lying horizontally on a flat solid surface results in the onset of subharmonic Faraday-like body waves, which is possible because earthworms have a hydrostatic skeleton with a flexible skin and a liquid-filled body cavity. Our findings are supported by theoretical analysis based on a model of parametrically excited vibrations in liquid-filled elastic cylinders using material parameters of the worm's body reported in the literature. The ability to excite nonlinear subharmonic body waves in a living organism could be used to probe, and potentially to control, important biophysical processes such as the propagation of nerve impulses, thereby opening up avenues for addressing biological questions of fundamental impact.

Vibrations and fluid-structure interactions are essential for efficient communication between living beings and they also underpin human-made imaging, spectroscopy and sensing techniques such as medical ultrasound and photoacoustic imaging modalities[1], Brillouin Light Scattering spectroscopy[2], and laser vibrometry[3] to name a few. Sound and vibrations are also likely to play an important role in the propagation of nerve impulses[4,5] as well as they can be used to develop new methods of bacteria and virus killing[6–8]. Furthermore, using vibrations one could monitor, understand and control the behaviour of some animals, such as earthworms[9], and exploit them to sense and modify soil structure as well as to increase crop yields[10–12].

Earthworms – tube-shaped, segmented worms that have a world-wide distribution and are commonly found in soil – have become a subject of intensive research focused on their response to vibrations and sound. Some of these studies aim to explain the response of these animals to natural vibrations produced by predators, rain or plants[9]. Furthermore, the glial cell wrapping of the giant axons of earthworms resembles the myelin sheath of vertebrate nerve fibers[13]. Therefore, earthworms serve as a platform for neurobiological studies[14]. Earthworms are also cheap and using them does not require ethics approval. Hence, we choose these animals to demonstrate the onset of Faraday-like subharmonic body waves in a living organism subjected to external mechanical vibration.

Classical nonlinear standing Faraday waves appear on the horizontal surface of an infinitely extended liquid supported by a vertically vibrating container[15]. For any given vibration frequency ω, when the vibration amplitude exceeds a certain critical value, the flat surface of the fluid becomes unstable and subharmonic surface waves oscillating at the frequency $\omega/2$ are formed. These oscillations are due to a parametric resonance between the forcing at the frequency ω and gravity-capillary surface waves with the dispersion relation $\Omega(k)$, being k a certain wave vector selected as $\Omega(k) = \omega/2$.

Faraday waves have become a paradigmatic example of nonlinear wave systems exhibiting complex periodic[16] and quasi-periodic[17–19] dynamics as well as chaotic behaviour[20–23]. Recently, a number of applications of Faraday waves in the fields outside the area fluid dynamics have been suggested, including novel photonic devices[24,25], metamaterials[26,27], alternative sources of energy[28], and applications in biology[29].

Parametrically excited vibrations and surface waves have also been observed in isolated liquid drops subjected to external mechanical forcing[30–38]. In response to vibration, the drop can either adopt a regular star shape[30–33] or exhibit a more dramatic transformation by spontaneously elongating in horizontal direction to form a worm-like structure of gradually increasing length[34–37].

[1]Centre for Micro-Photonics, Swinburne University of Technology, Hawthorn, Victoria, 3122, Australia. [2]Department of Mathematics, Faculty of Science Engineering and Technology, Swinburne University of Technology, Hawthorn, Victoria, 3122, Australia. e-mail: imaksymov@swin.edu.au; apototskyy@swin.edu.au

In contrast to the classical Faraday instability in infinitely extended systems, in isolated liquid drops the boundary conditions at the drop edge dictate the existence of a discrete set of vibrational modes[39–42]. The eigenfrequency Ω of each mode depends on the boundary conditions at the contact line[40,41]. When a drop is vibrated at the frequency ω, the fundamental subharmonic resonance occurs when the resonance condition $\Omega = \omega/2$ is fulfilled[30].

In inviscid fluids, the subharmonic response sets in at a vanishingly small vibration amplitude at frequencies that satisfy the resonance condition. For frequencies that do not satisfy the resonance condition, the critical amplitude is nonzero. In experiments with viscous isolated drops, the dependence of the subharmonic critical amplitude on the vibration frequency ω was shown to exhibit periodic variations[30,32,33]. This feature is in stark contrast with the Faraday instability in infinitely extended fluids, where the critical amplitude monotonically increases with the driving frequency ω[43].

In this work, we observe experimentally the subharmonic oscillations of the body of living earthworms lying horizontally on a flat solid surface subjected to vertical vibration. We measure the critical amplitude of the onset of subharmonic response as a function of the vibration frequency f, and we reveal that the obtained dependence exhibits signature characteristics of parametrically excited capillary surface waves in vibrated liquid drops[30–33]. In particular, we show that the critical amplitude varies periodically with f. We explain the observed results by modelling the body of the worm as a horizontally-extended, liquid-filled elastic cylinder subjected to vertical vibration.

Because the excitation of Faraday-like waves in living organisms has thus far received little attention[44], our findings promise to push the frontiers of our knowledge of fundamental nonlinear phenomena and chaotic behaviour in biological systems. For instance, our results should be qualitatively reproducible in other living systems such as bacteria, biological cells or individual organs in the body including the brain and blood vessels.

Experimental results

We tested four different earthworm species encountered in the south eastern regions of Australia[45]. To correctly identify the earthworm species, we used an earthworm identification guide[46]. *Eisenia fetida* earthworms were purchased from a local fishing goods store, and on average they were 100–120 mm long and 5–6 mm wide. *Lumbricus terrestris* earthworms were harvested in the field and closely related to them *Lumbricus rubellus* earthworms were obtained from a local compost worm supplier. In this group, we selected the worms that measured approximately 120–150 mm in length and 8–10 mm in width. Several smaller 6–8-mm-long and 2–3-mm-wide *Aporrectodea caliginosa* earthworms were also harvested in the field and outcomes of their test were qualitatively similar.

Earthworms are non-regulated animals, and therefore this research did not require the approval of our Institutional Animal Ethics Committee. However, the worms were treated as humane as practical and afterwards they were placed into a worm farm where they fully recovered.

In preparation for experiments, earthworms were first placed in 20% ethanol for approximately 2 minutes, which immobilised them to simplify handling. Then, the entire body of an immobilised worm was placed on top of a thin Teflon plate [Fig. 1(a)] that was vertically vibrated with the harmonic frequency f. The vibrations were detected by using an in-house laser vibrometry setup[38] [Fig. 1(b)] consisting of a red laser diode (Besram Technology, China, 650 nm wavelength and 1 mW maximum power) and a photodetector (Adafruit, USA). The intensity of light reflected from the worm is modulated due to the vertical vibration as well as the onset of parametrically excited body waves. We recorded these signals with Audacity software and Fourier-transformed them with Octave software to obtain frequency spectra. When required, the skin of the worm was moistened with water to avoid drying. However, in those cases special care was taken to remove all liquid drops from the Teflon plate. This ensured that Faraday waves are not excited on the liquid drop surface[38] and also dramatically simplified the analysis of the results.

The experiments were conducted by using the following protocol. The laser beam was focused on the body of the worm and the vibration amplitude of the Teflon plate was gradually increased until the point when the onset of Faraday instability was observed with the oscilloscope. The position of the worm was continually monitored with a digital camera to make sure that the same part of the worm is illuminated. Large vibration amplitudes leading to a horizontal displacement of the worm or jumps of the entire body were avoided to help keep the worm in the focus of the laser vibrometry setup. Large vibrations were also avoided because they additionally lead to ejection of a sticky fluid from the worm, which could serve as a medium for surface Faraday waves not wanted in our measurements. Typically, the total duration of measurements using the same worm was under five minutes to avoid desiccation. After the experiment, the worms were rehydrated and released into a worm farm.

Figure 2(a,b) show, respectively, the vibration spectrum of the Teflon plate without the worm and the vibration spectrum of a *Lumbricus terrestris* earthworm placed horizontally on top of the Teflon plate. In both cases the Teflon plate is subjected to vertical vibration at $f = 40$ Hz.

The vibration spectrum of the unloaded Teflon plate is dominated by the peak at the frequency $f = 40$ Hz and its higher-order harmonic frequencies 80, 120 and 160 Hz. The intensity of the second (third) harmonic is approximately 50 (80) times smaller than that of the fundamental signal and these signals are consistent with the intrinsic nonlinear distortion of the source of vertical vibrations used in our setup. We also calculated[47] that the fundamental natural vibration frequency of the Teflon plate is 43.7 Hz. The natural frequencies of the two higher order modes – 137.9 Hz and 294.9 Hz – are well above the vibration frequencies used in this work. This means that the vibration regime of the plate is far from the nearest anti-resonance and that its frequency response is uniform in the frequency range of interest.

In the vibration spectrum of the earthworm, we observe that the harmonic waves lose their stability via a period-doubling bifurcation[38] as evidenced by the appearance of the peaks at $f = 20$, 60, 140 and 180 Hz not present in the vibration spectrum of the Teflon plate. Significantly, the harmonic frequency peaks in the spectrum

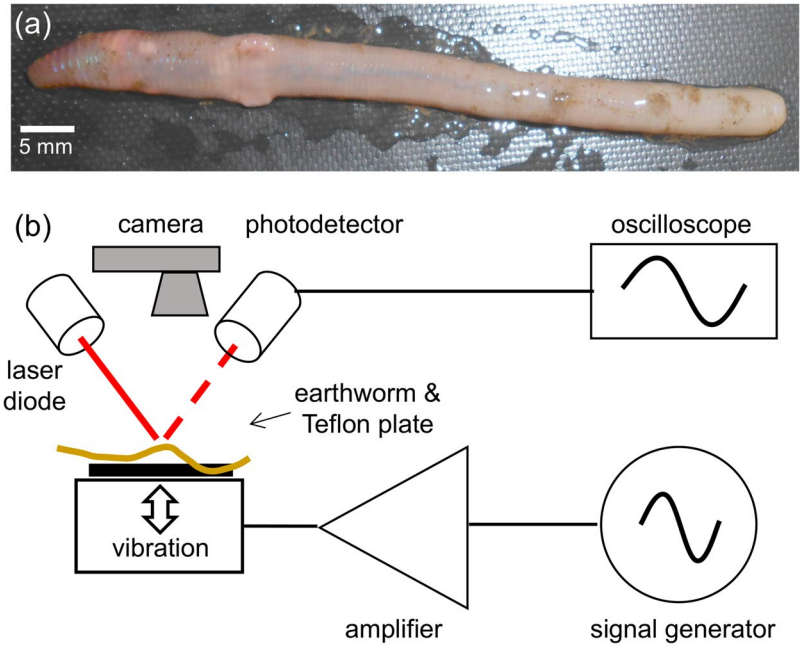

Figure 1. (**a**) Photograph of an anaesthetised *Eisenia fetida* earthworm. (**b**) Schematic of the experimental setup. A subwoofer covered by a thin Teflon plate is used as the source of vertical vibration. The sinusoidal vibration signal of frequency f is synthesised with a digital signal generator and amplified with an audio amplifier. Vibrations of the earthworm placed horizontally on top of the Teflon plate are measured by using a continuous wave red laser diode and a photodetector. The detected signals are visualised with an oscilloscope and sent to a laptop for post-processing. A digital camera is used to continuously monitor the position of the worm.

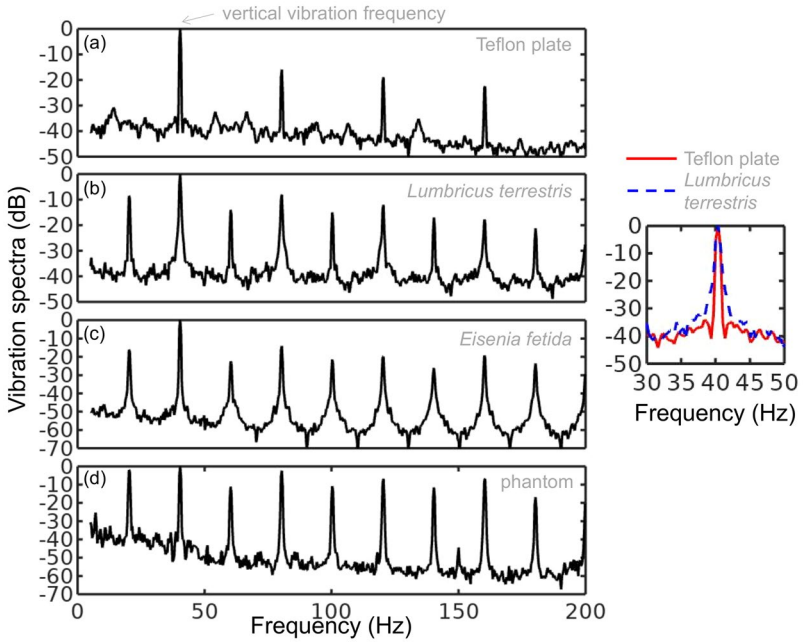

Figure 2. Vibration spectra of the (**a**) Teflon plate without the worm, (**b**) *Lumbricus terrestris* earthworm, (**c**) *Eisenia fetida* earthworm and (**d**) earthworm-mimicking phantom. The vertical vibration frequency is $f = 40$ Hz. All spectra are normalised to their respective maxima. Note the presence of subharmonic ($f/2$, $3f/2$ and so on) frequency peaks in the spectrum of the earthworms and the phantom, which are not present in the spectrum of the unloaded Teflon plate. The peaks in the spectrum of the earthworms are wider than in the case of the Teflon plate (as shown in the inset on the right), which is a result of the amplitude modulation and appearance of frequency sidebands leading to the broadening of the peak[38]. Also note that the spectra of the worms and the worm-mimicking phantom are qualitatively similar.

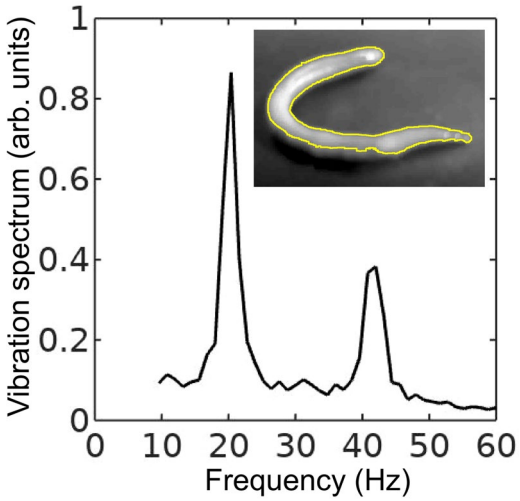

Figure 3. Vibration spectrum of the body of the earthworm subjected to vertical vibration at the frequency $f = 40$ Hz obtained by processing a video of the vibrated worm as explained in the main text. The subharmonic peak at $f/2 = 20$ Hz can be clearly seen. The inset shows an example of the contour of the worm obtained from a single frame extracted from the video.

of the worm are wider as compared with the respective peaks in the spectrum of the Teflon plate (see the right inset in Fig. 2). This is because the onset of subharmonic oscillations also results in the amplitude modulation and appearance of sidebands, which in turn leads to broadening of the spectral peaks previously reported for liquid films[20,21] and liquid drops subjected to vibration[38]. Qualitatively the same behaviour is observed in the vibration spectrum of the other tested earthworm species, including the *Eisenia fetida* worms [Fig. 2(c)]. We also note that the observed broadening effect cannot be attributed to the response of the Teflon plate. In general, broadening of spectral peaks of vibrated solid bodies can only be observed in the regime of extremely large vibration amplitudes not reached in our experiments.

Experimental idealisation of a worm as an elongated liquid drop covered by a thin elastic skin is feasible because their water-filled body cavity is surrounded by a flexible skin and it acts as a hydrostatic (i.e. supported by fluid pressure) skeleton[48]. The muscles of the worm are made of a viscoelastic material, but their volume is small as compared with that of the water-like liquid inside the body of the worm. Yet, when the worm is anaesthetised, its nervous system does not produce nerve impulses and therefore the muscles of its body are fully relaxed[14]. Consequently, the viscoelastic properties of the muscles can be neglected in the analysis of anaesthetised worms. Furthemore, whereas in non-anaesthetised worms high internal pressure helps to maintain a cylindrical shape[49], the pressure in anaesthetised worms is close to ambient[50]. We verified this by establishing that a puncture of the skin of an anaesthetised worm does not lead to a dramatic ejection of internal fluids typically seen in non-anaesthetised worms. (Here, we draw an analogy between the worm and a pressurised balloon).

To verify that an anaesthetised worm can be experimentally idealised as a water drop at ambient pressure enclosed by a thin elastic skin, we tested an earthworm-mimicking phantom made of a finger of an approximately 0.1-mm-thick latex glove filled with water. The thickness of the phantom wall is of the same order of magnitude as the body wall of an earthworm[51], but mechanical properties of latex films of sub-millimeter thickness[52] are similar to those of living worms[53]. The vibration spectrum of the phantom is shown in Fig. 2(d) and it is in good qualitative agreement with the vibration spectra of the real earthworms.

Furthermore, in the following we assume that the body wall of the worm is an elastic cylindrical shell undergoing flexural vibrations. (A relevant model was used in ref. [12], but later on in this paper we show that flexural vibrations should be responsible for the subharmonic response of the worms). Direct mapping of flexural vibration modes with our laser vibrometry setup is currently unavailable. Thus, to demonstrate that the entire body of worm undergoes vibrations resulting in the appearance of subharmonic frequencies in the vibration spectrum, we use a time-domain approach. We first film worms vibrated at 40 Hz frequency with a digital camera capturing 120 frames per second and then we process the resulting videos in Octave software, where we binarise each frame and use the `bwboundaries` command to find the contours of the worm (see the inset in Fig. 3). Then, we calculate the area of the contour for every frame and we finally Fourier-transform the resulting area-versus-time dependence to obtain the vibration spectrum of the body of the worm.

As shown in Fig. 3, in agreement with the results obtained with the laser vibrometry setup (Fig. 2), the body of the worm oscillates at the vibration frequency $f \approx 40$ Hz and the subharmonic frequency $f/2 = 20$ Hz. However, whereas the spectra in Fig. 2 were obtained by focusing the laser beam on a part of the worm's body, the spectrum in Fig. 3 originates from the vibrations of the entire body of the worm. The higher frequencies peaks present in Fig. 2 are not reproduced in Fig. 3, because the finite resolution and sample rate of the digital camera limit the resolving ability of the image processing based approach at higher frequencies.

As a next step, we measure the lowest value of the vibration amplitude at which the subharmonic response of the worm body sets in. We call this value the critical amplitude and we plot it in Fig. 4 as a function of the

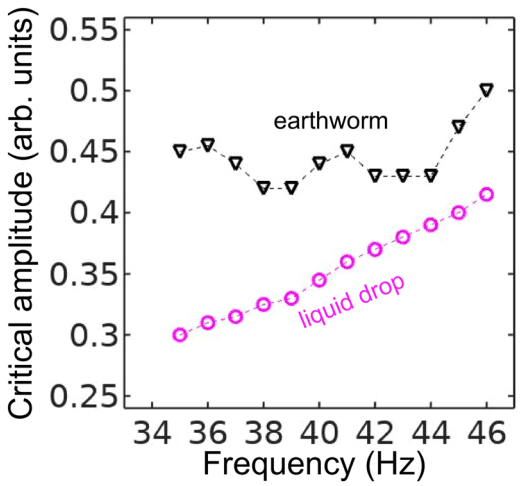

Figure 4. Critical vibration amplitude of the onset of the subharmonic response in an earthworm (triangles) and a pancake-like canola oil drop (circles) plotted as a function of the vertical vibration frequency *f*. The dashed lines are the guide to the eye. Whereas in the selected frequency range the response of the canola oil drop is quasi-monotonic, the curve for the critical amplitude for the worm exhibits oscillations. These oscillations allow us to correlate the experimental data with the predictions of our theoretical model.

frequency f for an *Eisenia fetida* worm. To obtain consistent results, we illuminated the same part of the body of the worm and we also established that the critical amplitude was unaffected by the intensity of the laser beam and the diameter of the laser spot. Significantly, in the investigated frequency range, the response of the Teflon plate to vertical vibrations is essentially uniform within the margin of error and also it is linearly proportional to the acoustic response of the subwoofer. The amplifier of the subwoofer also operates in the linear regime that allows us to use its input as a measure of the vibration amplitude. Thus, the measured critical amplitude is based on the input of the subwoofer, it does not require normalisation on the response of the Teflon plate and therefore its variations with the frequency are attributed solely to the response of the worm.

In the 35…45 Hz frequency range, the critical amplitude is relatively low and therefore the body of the worm does not shift along the surface of the Teflon plate, thereby allowing us to obtain accurate results. In the critical amplitude dependence for the worm (Fig. 4), we observe oscillations with the two minima at $f \approx 38$ Hz and $f \approx 43$ Hz. In contrast, the critical amplitude of an approximately 6×6 cm pancake-like drop of canola oil is quasi-monotonic in the 35…45 Hz range. [However, in agreement with the previous results[30,32,33], we observed a non-monotonic response at $f > 50$ Hz (not shown for simplicity)].

A similar nonmonotonic dependence of the critical amplitude on the vibration frequency was previously observed in infinitely extended viscoelastic films[54]. In contrast to liquid drops of simple Newtonian fluids[38], the nonmonotonic dependence originates from the ability of a viscoelastic material to'remember' past stresses. Thus, in the Maxwell model of linear elasticity, the instantaneous stress in the material is described by a time-dependent relaxation modulus decaying over a characteristic relaxation time. The coupling between the period of forcing with the relaxation time of the material viscoelastic response leads to the oscillation of the critical amplitude as the function of the vibration frequency.

Based on our experimental data, it is not possible to conclude whether the nonmonotonic dependence in Fig. 4 is due to viscoelastic properties of the skin of the worm, the finite size of the worm body or a combined effect of viscoelastic properties of the skin and the geometry of the worm. In the following, we assume that, similar to small liquid drops[30–33], the nonmonotonic subharmonic response of the worm originates from the discrete spectrum of its natural vibration frequencies. We also develop a theoretical model considering the worm as an elastic cylindrical shell filled with an incompressible fluid, and we correlate the experimental results with the theoretical predictions.

Theoretical model

The observed subharmonic oscillations of the earthworms bear a striking resemblance to the well-known phenomenon of parametrically excited capillary surface waves in vertically vibrated liquid drops[30–33,55]. To understand the physical origin of the subharmonic response of earthworms, we neglect the damping effect of the viscosity and model the body wall of the worm as an elastic cylindrical shell of length L with the Young's modulus E, radius R and shell thickness H. The cylinder is filled with incompressible and inviscid fluid with the density ρ_l.

An elastic cylindrical shell model of the worm body has been previously used to analyse the pressure exerted by earthworms during their burrowing activity[12]. When such a cylinder with the horizontally oriented axis is supported by a solid plate, its cross-sectional shape is no longer circular due gravity deformation [Fig. 5(left)]. To estimate the squashing depth δ that measures the change in the vertical height of the cylinder in the squashed state, we neglect the bending energy of the thin shell ($h \ll R$) as compared with the energy due to stretching. In this case, the equilibrium shape of the gravity deformed cross-section of the cylinder filled with an incompressible fluid of density ρ_l can be found by bal-

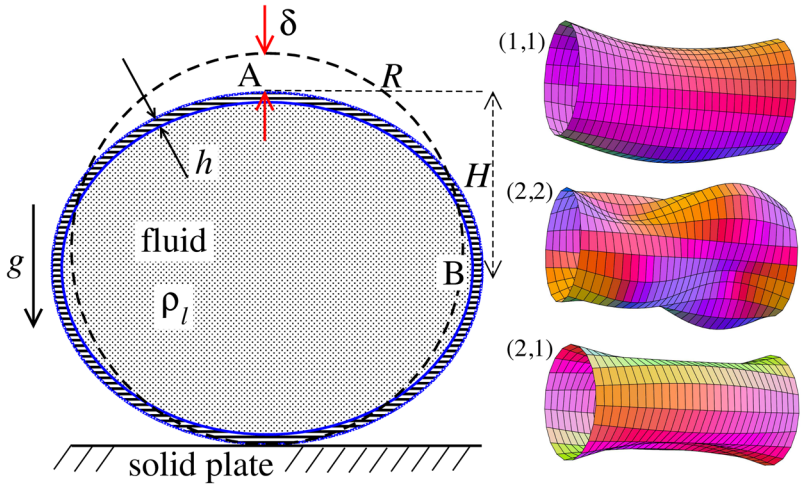

Figure 5. Schematic of the theoretical model for a vibrated earthworm represented as a liquid-filled elastic cylinder of length L with the Young's modulus E, undeformed radius R, and shell thickness h. The cylinder is filled with incompressible and inviscid fluid with the density ρ_l. (left) Cross-section of the elastic cylinder deformed by the gravity in contact with a non-deformable solid plate. The dashed line shows the contour of an undeformed cylinder of radius R. The squashing depth is $\delta \approx R\sqrt{\rho g R^2/(3Eh)}$. (right) Calculated spatial profiles of the first three lowest frequency vibration modes. The integer numbers in the parentheses denote, respectively, the number of the circumferential and the axial vibration mode (see the main text).

ancing the tension T per unit axial length of the elastic shell with the hydrostatic pressure[56]. In particular, we obtain $\rho_l g H = T(\kappa_B - \kappa_A)$, where H is the height difference between the points A and B in Fig. 5 (left) and $\kappa_{A,B}$ denotes the curvature of the shell at the points (A, B). Assuming weak deformation such that $\delta/R \ll 1$, we approximate the shape of the squashed cylinder by an ellipse with the minor and the major semi-axis $R - \delta/2$ and $R + \delta/2$, respectively. Then, the curvatures to the first order in δ/R are $\kappa_A = (R - \delta/2)/(R + \delta/2)^2 \approx R^{-1} - 3\delta/(2R^2) + O(\delta/R)^2$ and $\kappa_B = (R + \delta/2)/(R - \delta/2)^2 \approx R^{-1} + 3\delta/(2R^2) + O(\delta/R)^2$. Finally, taking into account that $T = Eh\delta/R$ and $H = R - \delta/2$, we obtain the following estimate

$$\frac{\delta}{R} = \sqrt{\frac{\rho g R^2}{3Eh}}. \tag{1}$$

Viscoelastic properties of earthworms are poorly understood and previous works on mechanical properties of earthworms worm do not report the values of the Young's modulus[57,58]. However, mechanical properties of millimeter-sized nematode *Caenorhabditis elegans* worms have been recently reported[53], where a micropipette deflection setup[59] was used to study the stiffness of the worms. In particular, the effective bulk Young's modulus of the worm body was found to be in the $10^5 \ldots 10^6$ Pa range, with the maximum value originating from the cuticle. On the other hand, it has also been suggested that all nematodes exhibit a universal elastic response dominated by the mechanics of pressurised internal organs[60]. Nevertheless, the values of the bulk modulus reported in[60] are of the same order of magnitude as those in ref. [53]. Furthermore, the effective Young's modulus of the cuticle strongly depends on its thickness[53,60]. Thus, assuming that the elasticity of the worm body is entirely due to the stiffness of the cuticle, the Young's modulus can reach 200…400 MPa[61].

Significantly, for the lowest expected value of the effective Young's modulus of the cuticle $E = 1$ MPa[53,60] the gravity squashing of the worm body remains small, as demonstrated below. We take the thickness of the cylindrical wall to be $h = 50$ μm, which corresponds to the combined thickness of the cuticle and the epidermis of earthworms[51]. The effective density of the internal body fluid can be estimated as $\rho_l = 1100$ kg/m^3 because the body of the worm consists of a water-like liquid[48] and it also contains blood vessels filled with blood, where the density of blood plasma is approximately 1025 kg/m^3 and the density of blood cells circulating in the system is approximately 1125 kg/m^3. Finally, for the largest possible value of the worm radius used in our experiments $R = 5$ mm, we estimate the relative squashing from Eq. (1) to be $(\delta/R) \approx 4\%$. We note that in reality (δ/R) should be much smaller than 4% because the effective Young's modulus of the cuticle could be about three orders of magnitude higher[61].

Then, we neglect viscoelastic damping and obtain a linear model of parametrically excited subharmonic body waves in an elastic fluid-filled cylinder. We follow the approach developed for subharmonic vibrations of a water drop placed on an oscillating solid plate[30], where natural vibration frequencies of a cylinder squashed by gravity are considered [Fig. 5(left)]. The degree of squashing is characterised by the indentation depth δ that, in turn, is proportional to the gravity acceleration g. In the co-moving frame of the vibrating plate, the gravity is time-dependent. This means that the effect of the vibration is equivalent to periodically varying the squashing of the cylinder. Therefore, in the linear regime, natural frequencies of the squashed cylinder are periodically modulated, thereby leading to a parametric type of forcing.

To the best of our knowledge, the analysis of the vibrational frequencies of a cylinder supported by a solid plate along its entire length has not been reported. (Although Faraday instability of a horizontal water-filled half-cylinder subjected to vertical vibrations was investigated in a recent work[55], the model presented there cannot be applied in our case because it does not consider mechanical properties of the earthworm skin). Therefore, we estimate the order of magnitude of the natural frequencies by using the well-known result for a cylinder with freely supported ends[62–64], as demonstrated below. A comprehensive review of the linear and nonlinear vibration and instabilities of cylindrical shells and plates can be found in refs. [47,65,66].

In cylindrical coordinates, the axial $u(r,\ \theta)$, azimuthal $v(r,\ \theta)$ and radial $w(r,\ \theta)$ displacements of the shell of a cylinder with freely supported ends can be written as

$$\begin{aligned} u &= U(t)\cos(\pi mz/L)\cos(n\theta), \\ v &= V(t)\sin(\pi mz/L)\sin(n\theta), \\ w &= W(t)\sin(\pi mz/L)\cos(n\theta), \end{aligned} \tag{2}$$

where the integers n and m determine the circumferential and the axial vibration modes, respectively. As a representative example, in Fig. 5(right) we show the first three lowest frequency modes.

For $\delta/R \ll 1$, the deviation of vibrational frequencies from those of a circular cylinder is of first order in δ/R[67]. This allows us to write the equations of motion for the amplitudes $U,\ V,\ W$ as

$$\ddot{\boldsymbol{x}} \approx \left(\boldsymbol{J}_0 + \frac{\delta}{R}\boldsymbol{J}_1\right)\boldsymbol{x}, \tag{3}$$

where $\boldsymbol{x} = (U,\ V,\ W)$, $\boldsymbol{J}_0$ is the Jacobi matrix corresponding to the circular cylinder and $\boldsymbol{J}_1$ is its first order correction due to squashing. When the solid plate is vibrated with the frequency ω, its vertical displacement is given by $A\cos(\omega t)$, where A is the vibrational amplitude. The gravity acceleration in the co-moving frame of reference is $g(t) = g[1 + a\cos(\omega t)]$, where $a = A\omega^2/g$ is the dimensionless scaled amplitude. Since viscosity is neglected, we anticipate the onset of the subharmonic vibrations at small amplitude $a \ll 1$. In this regime, we obtain from Eq. (1) for the time-dependent squashing $\delta/R \approx \sqrt{\frac{\rho gR^2}{3Eh}}\left(1 + \frac{a}{2}\cos\left(\omega t\right)\right)$. In this limit, Eq. (3) reduces to the three-dimensional Mathieu equation

$$\ddot{\boldsymbol{x}} = \left(\boldsymbol{J}_0 + \sqrt{\frac{\rho gR^2}{3Eh}}\boldsymbol{J}_1 + q\cos(2\pi f)\boldsymbol{J}_1\right)\boldsymbol{x}, \tag{4}$$

where $q = \frac{a}{2}\sqrt{\frac{\rho gR^2}{3Eh}}$ is the scaled vibration amplitude.

We emphasise that the linear model Eq. (4) can only be used for qualitative estimations of generally nonlinear subharmonic response. Discrepancies with experimental results obtained for real earthworms can be due to viscoelastic damping, nonlinear deformation and twisting of the worm body, as well as due to the assumption of a thin wall elastic cylinder filled with Newtonian fluid used in the model.

The properties of solutions of Eq. (4) are well-known[68]. Parametrically excited instability sets in when $2\pi f$ coincides with one of the combination frequencies $|(\omega_0)_i \pm (\omega_0)_k|$, where $(\omega_0)_i^2\ (i = 1,\ 2,\ 3)$ are the eigenvalues of $-(\boldsymbol{J}_0 + \sqrt{\frac{\rho gR^2}{3Eh}}\boldsymbol{J}_1)$. Because $\sqrt{\frac{\rho gR^2}{3Eh}} \sim 0.04$ for $E = 1$ MPa, we can neglect the term $\sqrt{\frac{\rho gR^2}{3Eh}}\boldsymbol{J}_1$ in Eq. (4) as compared with $\boldsymbol{J}_0$, which implies that the natural frequencies $(\omega_0)_i$ of the gravity squashed worm can be approximated by those of a circular elastic cylinder.

Amongst the three frequencies $(\omega_0)_i\ (i = 1,\ 2,\ 3)$ one is typically two orders of magnitude lower than the other two. This lowest frequency ω_0 corresponds to the mode with predominantly radial displacement and is given by[64]

$$\frac{\omega_0^2R^2\rho}{E} = \left(\frac{h^2(\lambda_m^2 + n^2)^2}{12R^2(1 - \nu^2)} + \frac{\lambda_m^4}{(\lambda_m^2 + n^2)^2}\right)\left(1 + \frac{a\rho_l I_n(\lambda_m)}{\lambda_m h\rho(I_n)'(\lambda_m)}\right)^{-1}, \tag{5}$$

where $\lambda_m = m\pi R/L$ and I_n is the modified Bessel function of the first kind of order n.

Considered as a whole, the combination $\omega_0 R\sqrt{\frac{\rho}{E}}$ in Eq. (5) (called the frequency factor) depends on the geometry of the cylinder, the Poisson ratio ν and the ratio of the densities ρ_l/ρ, but is independent of the Young's modulus E. In Fig. 6(a), we plot the frequency factor as a function of the axial mode number m for different values of n for a cylinder of length $L = 10$ cm, shell thickness $h = 50\ \mu$m, radius $R = 5$ mm, filled with a fluid with density $\rho_l = \rho = 1100$ kg/m^3. The first three lowest frequency modes with $(n = 1,\ m = 1)$, $(n = 2,\ m = 2)$ and $(n = 2,\ m = 1)$ are shown in the right panel of Fig. 5 for the sake of illustration.

Discussion

The presented theoretical model can, in general, be used to find the mode profiles corresponding to the resonance frequencies found in the experiment in Fig. 4 by using experimental data for the Young's modulus E of earthworms as a key input parameter. However, plausible values of E for different worm species are a subject of active debate due to a large range of the reported values and poor understanding of the impact of the cuticle on mechanical properties of worms[53,60].

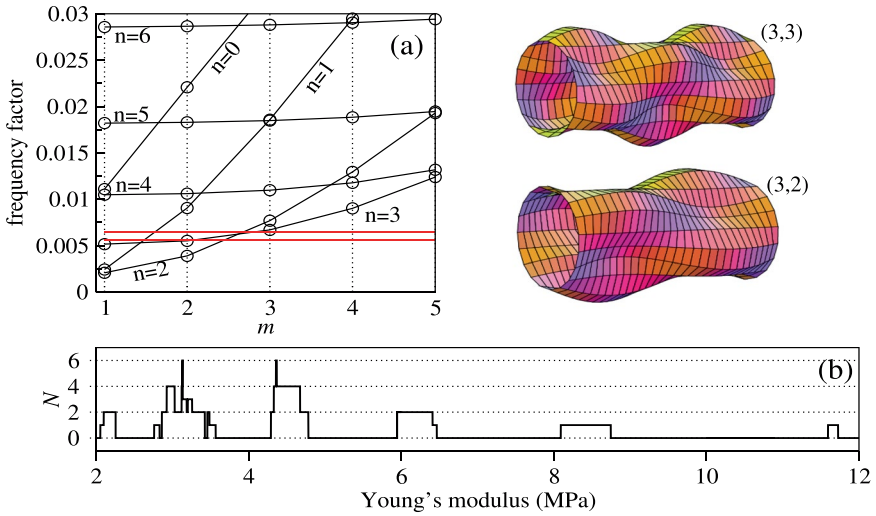

Figure 6. Analysis of experimental results in light of the predictions of the developed theoretical model. By scanning through all theoretically possible combinations of vibration modes and varying the value of the effective Young's modulus of the worm, we find the modes involved in the subharmonic response of the worm and plot the respective spatial mode profiles. (**a**) Frequency factor $\omega_0 R\sqrt{\rho/E}$ plotted as a function of the axial mode number m for the circular elastic cylinder filled with liquid with density ρ_l. The other parameters are $R = 5$ mm, $L = 10$ cm, $\rho = \rho_l = 1100\,\mathrm{kg/m^3}, \nu = 0.5$ and $h = 50\,\mu$m. The circumferential mode number n is indicated next to each curve. The two solid horizontal lines correspond to the levels of $38\pi R\sqrt{\rho/E}$ and $43\pi R\sqrt{\rho/E}$ with $E = 8.3$ MPa. For $E = 8.3$ MPa, the mode $(n = 3,\ m = 3)$ is excited at 38 Hz and the mode $(n = 2,\ m = 3)$ is excited at 43 Hz. The frequencies 38 Hz and 43 Hz correspond to the first and the second minimum of the critical vibration amplitude function in Fig. 4. (**b**) The number of modes N that match the subharmonic resonance criterion as a function of E (see the main text for details). From this panel we obtain information about the largest possible values of the Young's modulus corresponding to the modes at 38 Hz and 43 Hz.

To circumvent the lack of experimental data, we reanalyse our experimental results in Fig. 4 in light of the predictions of the developed model Eqs. (4 and 5). In particular, we establish which of the theoretically possible vibrational modes could be excited at a given value of E. Here, we vary the value of E in a range bounded by two critical values – the effective bulk Young's modulus of the worm from ref. [53] and the locally measured stiffness of the cuticle[60,61]. Whereas the exact values of E are yet to be confirmed experimentally, it has already been established that E would be a function of the thickness of the cuticle[60] and that it would approach 200…400 MPa[61] in a limiting case of the mechanical properties of the worm defined solely by the cuticle.

Naturally, the thickness and stiffness of the cuticle vary for different species of worms and they are also likely to vary from one animal to another within the same species group. Indeed, in our experiments we established that *Eisenia fetida* earthworms appear to be slightly stiffer when palpated as compared with the other species tested in this work. However, this difference alone cannot result in an order of magnitude discrepancy in the values of E.

Firstly, for the fundamental subharmonic resonance in our model we choose the doubled frequency to be $\omega_0 = \pi f_{\min}$, where $f_{\min}$ is either 38 Hz or 43 Hz corresponding to the first and the second minimum of the measured critical vibration amplitude function (Fig. 4). Then, for any fixed value of E we find all theoretically possible vibrational modes $(n = 0, \ldots, m = 1, \ldots)$ whose doubled frequency ω_0/π differs by at most 1 Hz from either 38 Hz or 43 Hz. We choose the tolerance of ± 1 Hz because it corresponds to the frequency resolution in the experimental data in Fig. 4. It is noteworthy that our model predicts another upper bound for E when the tolerance is varied. However, choosing the tolerance dictated by the resolution in the experimental data serves the purpose of comparing the experimental and theoretical results obtained in this work.

Denoting the number of modes that match 38 Hz and 43 Hz as N_{38} and N_{43}, respectively, we define the total number of matches as $N = N_{38}N_{43}$. Finally, by gradually varying E with a fixed increment, we obtain the dependence $N(E)$ and plot it in Fig. 6(b). We observe that the largest possible value of the Young's modulus lies in the $E = 8.3\ldots8.9$ MPa range, which corresponds to the mode $(n = 3,\ m = 3)$ excited at $f = 38$ Hz and the mode $(n = 2,\ m = 3)$ excited at $f = 43$ Hz. The corresponding values of the frequency factor are shown by the two horizontal lines in Fig. 6(a). Based on these results, we predict that the body of the worm subjected to vertical vibration and undergoing Faraday-like body oscillations would assume the spatial profiles shown in the insets in Fig. 6(a).

The values of the Young's modulus $E = 8.3\ldots8.9$ MPa produced by our model feasibly fall within the expected range. In fact, these values are approximately one order of magnitude higher than those of the effective bulk Young's modulus of the worm predicted in ref. [53], being at the same time one order of magnitude lower than those obtained from local measurements of the stiffness of the cuticle[60,61]. This is consistent with the point of view that the effective mechanical properties of the worm are not exclusively defined by the stiffness of the cuticle. However, we also conclude that the cuticle plays a considerable role in the response of the worm to vibration.

Conclusions

We have demonstrated the excitation of subharmonic Faraday-like waves in living earthworms lying horizontally on a flat solid surface subjected to vertical vibration. We tested four common species of earthworm – *Eisenia fetida*, *Lumbricus terrestris*, *Lumbricus rubellus* and *Aporrectodea caliginosa*, and in all tests we observed the appearance of spectral peaks at subharmonic frequencies with overall behaviour similar to that of finite-size liquid drops subjected to vibration. We also used an earthworm-mimicking phantom made of a water-filled cylinder with thin elastic walls, the measurements of which qualitatively reproduced the response of the real earthworms. Moreover, we measured the critical amplitude of the onset of subharmonic waves in the worms and found that it exhibits oscillations as a function of the driving frequency. This feature is typically observed in the response of infinitely extended viscoelastic fluids[54] and isolated small drops composed of a Newtonian fluid[30–33]. By modelling the body of the worm as an elastic cylindrical shell filled with fluid, we explained the observed subharmonic response by parametric excitation of the discrete set of vibrational modes. We therefore conclude that the nonmonotonic dependence of the critical amplitude on the vibration frequency should be a direct consequence of the discrete nature of the spectrum of eigenfrequencies.

Because biological cells and many living organisms are mostly made of fluids, unique properties of nonlinear waves observed in fluidic systems are likely to open up unique opportunities for biology and medicine as well as the adjacent areas. The work in this direction is already in progress[44,55]. Thus, we believe that our results would not only push the frontiers of our knowledge of fundamental nonlinear phenomena and chaotic behaviour in biological systems, but they could also be used to develop new techniques for probing and controlling biophysical processes inside a living body.

For example, it has been suggested[69] that Faraday-like body waves in vibrated living earthworms could be used to verify the soliton model of nerve pulse propagation[4,5]. Mechanical stimulation has long been used to excite nerve impulses[70], but so far this has not enabled researchers to establish a reliable link with the brain. The ability to form a soliton in the nerve may not necessarily mean that solitons underpin the principal natural mechanism for nerve impulse propagation. However, the demonstration of soliton existence in externally excited nerve fibres would be a paradigm shift in the way we understand the nervous system[4,5]. As shown in this paper, Faraday-like body waves in living earthworms may have 20–300 Hz frequencies coinciding with those of natural nerve impulses. Thus, hypothetically, constructive or destructive interference of these waves with nerve impulses could be used to amplify or suppress the nerve signalling in a living worm[69], which in turn should open up novel opportunities to control nerve signals mechanically.

Finally, we note that in neuroscience experiments the worm is often anaesthetised to inhibit the generation of natural nerve impulses[14]. We experimented with non-anaesthetised and lightly sedated worms and we also observed the onset of Faraday-like body waves in many cases. However, whereas this result indicates that the results presented in our work should also apply to non-anaesthetised worms, it is very challenging to keep the worms in the focus of the laser beam and therefore experimental data are difficult to interpret and analyse using the available mathematical models.

We also note that our theoretical model remains valid in case of non-anaesthetised earthworms having higher internal pressure. As a result, the linear approximation Eq. (4) neglecting the squashing depth becomes even more accurate because the squashing depth in Eq. (1) is further decreased. Because natural frequencies of pressurised elastic cylinders increase as compared with those of low-pressure elastic cylinders[71], in non-anaesthetised earthworms the minima in the critical vibration amplitude in Fig. 4 should shift to higher frequencies.

Methods

The hardware used in our experimental setup is similar to that in[38]. Because the maximum frequency of interest in this work is about 200 Hz, we used a photodiode (Adafruit, USA) designed for general applications in sensors and laboratory instrumentation. The photodiode is sensitive to the light in the broad 400…1100 nm spectral range with the sensitivity peak around 750 nm. The maximum frequency response of the photodiode measured using our laser diode controlled by an electronic driver circuit is 14 kHz, which is well above 200 Hz. Photodetector data were acquired using Audacity, a standard digital audio recording software that is often used for research purposes[14]. Overall, at low vibration frequencies and other similar experimental conditions, the accuracy of our setup is comparable to that of a commercial laser Doppler vibrometer.

Because of the low vibration frequencies, a consumer action camera (Kogan 4K, Australia) providing the resolution of 1280×720 pixels at 120 FPS speed was able to resolve the frequencies of the harmonic and subharmonic response of the body of the earthworm. Moreover, this camera is waterproof and easy to clean, which is important in research on animals, and it is also equipped with a 140° wide lens that allows capturing more ambient light, thereby dramatically improving the resolution as compared with a standard high-speed digital camera recording at up to 1000 FPS at the same illumination conditions.

Data produced by the camera were processed using the FFmpeg and Octave software. Because in all experiments our setup operated in a regime of moderate vibration amplitudes, approximately 30-second-long videos of vibrated worms were not affected by significant motion of the worm with respect to the centre of the camera's field of view. Long worms were bent to maximise the portion of their body captured by the camera. However, the curvature of the worm's body did not affect the results of our analysis. Because all liquids surrounding the worm were carefully removed before each measurement using a syringe and cotton wool tips, the standard Octave command `bwboundaries` alone allowed finding the contours of the worm without the need of removing artefacts.

Data availability

The datasets generated during and/or analysed during the current study are available from the corresponding author on reasonable request.

Received: 23 February 2020; Accepted: 28 April 2020;
Published online: 22 May 2020

References

1. Emelianov, S. Light, sound, nanobubbles: New approach to contrast-enhanced ultrasound and photoacoustic imaging. *J. Acoust. Soc. Am.* **145**, 1779–1779 (2019).
2. Ballmann, C. W., Meng, Z. & Yakovlev, V. V. Nonlinear brillouin spectroscopy: what makes it a better tool for biological viscoelastic measurements. *Biomed. Opt. Express* **10**, 1750–1759 (2019).
3. Blamey, J., Yeo, L. Y. & Friend, J. R. Microscale capillary wave turbulence excited by high frequency vibration. *Langmuir* **29**, 3835–3845 (2013).
4. Heimburg, T. & Jackson, A. D. On soliton propagation in biomembranes and nerves. *PNAS* **102**, 9790–9795 (2005).
5. Hady, A. E. & Machta, B. B. On soliton propagation in biomembranes and nerves. *Nat. Commun.* **6**, 6697 (2015).
6. Zinin, P. V., Allen, J. S. III & Levin, V. M. The mechanical resonances of bacteria cells. *Phys. Rev. E* **72**, 61907 (2005).
7. Ivanova, E. P. *et al*. Bactericidal activity of black silicon. *Nat. Commun.* **4**, 2838 (2013).
8. Boyd, B., Suslov, S. A., Becker, S., Greentree, A. D. & Maksymov, I. S. Beamed UV sonoluminescence by aspherical air bubble collapse near liquid-metal microparticles. *Sci. Reps.* **10**, 1501 (2020).
9. Mitra, O., Callaham, M. A., Smith, M. L. & Yack, J. E. Grunting for worms: seismic vibrations cause *Diplocardia* earthworms to emerge from the soil. *Biol. Lett.* **5**, 16–19 (2008).
10. Blakemore, R. & Hochkirch, A. Restore earthworms to rebuild topsoil. *Nature* **545**, 30 (2017).
11. Lacoste, M., Ruiz, S. & Or, D. Listening to earthworms burrowing and roots growing-acoustic signatures of soil biological activity. *Sci. Reps.* **8**, 10236 (2018).
12. Ruiz, S. A. & Or, D. Biomechanical limits to soil penetration by earthworms: direct measurements of hydroskeletal pressures and peristaltic motions. *J. R. Soc. Interface* **15**, 20180127 (2018).
13. Roots, B. I. & Lane, N. J. Myelinating glia of earthworm giant axons: Thermally induced intramembranous changes. *Tissue Cell* **15**, 695–509 (1983).
14. Shannon, K. M., Gage, G. J., Jankovic, A., Wilson, W. J. & Marzullo, T. C. Portable conduction velocity experiments using earthworms for the college and high school neuroscience teaching laboratory. *Adv. Physiol. Educ.* **38**, 62–70 (2014).
15. Faraday, M. On a peculiar class of acoustical figures; and on certain forms assumed by groups of particles upon vibrating elastic surfaces. *Philos. Trans. Royal Soc* **121**, 299–340 (1831).
16. Benjamin, T. B., Ursell, F. J. & Taylor, G. I. The stability of the plane free surface of a liquid in vertical periodic motion. *Proc. Royal Soc. Lond. A* **225**, 505–515 (1954).
17. Henderson, D. M. & Miles, J. W. Single-mode faraday waves in small cylinders. *J. Fluid Mech.* **213**, 95–109 (1990).
18. Miles, J. W. Nonlinear Faraday resonance. *J. Fluid Mech.* **146**, 285–302 (1984).
19. Jiang, L., Ting, C.-L., Perlin, M. & Schultz, W. W. Moderate and steep faraday waves: instabilities, modulation and temporal asymmetries. *J. Fluid Mech.* **329**, 275–307 (1996).
20. Punzmann, H., Shats, M. G. & Xia, H. Phase randomization of three-wave interactions in capillary waves. *Phys. Rev. Lett.* **103**, 064502 (2009).
21. Xia, H., Maimbourg, T., Punzmann, H. & Shats, M. Oscillon dynamics and rogue wave generation in faraday surface ripples. *Phys. Rev. Lett.* **109**, 114502 (2012).
22. Shats, M., Punzmann, H. & Xia, H. Capillary rogue waves. *Phys. Rev. Lett.* **104**, 104503 (2010).
23. Shats, M., Xia, H. & Punzmann, H. Parametrically excited water surface ripples as ensembles of oscillons. *Phys. Rev. Lett.* **108**, 034502 (2012).
24. Tarasov, N., Perego, A. M., Churkin, D. V., Staliunas, K. & Turitsyn, S. K. Mode-locking via dissipative faraday instability. *Nat. Commun.* **7**, 12441 (2016).
25. Huang, S.-W. *et al*. Multispectral optical frequency comb based on microresonator faraday instability. In *Frontiers in Optics 2017*, FTu5A.3 (Optical Society of America, 2017).
26. Domino, L., Tarpin, M., Patinet, S. & Eddi, A. Faraday wave lattice as an elastic metamaterial. *J. Appl. Phys.* **93**, 050202(R) (2016).
27. Francois, N., Xia, H., Punzmann, H., Fontana, P. & Shats, M. Wave-based liquid-interface metamaterials. *Nat. Commun.* **8**, 14325 (2017).
28. Alazemi, S., Lacarbonara, W. & Daqaq, M. F. Harvesting energy from Faraday waves. *J. Appl. Phys.* **122**, 224501 (2017).
29. Sheldrake, M. & Sheldrake, R. Determinants of Faraday wave-patterns in water samples oscillated vertically at a range of frequencies from 50–200 Hz. *Water* **9**, 1–27 (2017).
30. Yoshiyasu, N., Matsuda, K. & Takaki, R. Self-induced vibration of a water drop placed on an oscillating plate. *J. Phys. Soc. Jpn.* **65**, 2068–2071 (1996).
31. Noblin, X., Buguin, A. & Brochard-Wyart, F. Vibrations of sessile drops. *Eur. Phys. J. Spec. Top.* **166**, 7–10 (2009).
32. Ma, X., Liétor-Santos, J.-J. & Burton, J. C. Star-shaped oscillations of leidenfrost drops. *Phys. Rev. Fluids* **2**, 031602 (2017).
33. Ma, X. & Burton, J. C. Self-organized oscillations of leidenfrost drops. *J. Fluid Mech.* **846**, 263–291 (2018).
34. Hemmerle, A., Froehlicher, G., Bergeron, V., Charitat, T. & Farago, J. Worm-like instability of a vibrated sessile drop. *EPL (Europhys. Lett.)* **111**, 24003 (2015).
35. Pucci, G., Fort, E., Ben Amar, M. & Couder, Y. Mutual adaptation of a Faraday instability pattern with its flexible boundaries in floating fluid drops. *Phys. Rev. Lett.* **106**, 024503 (2011).
36. Pucci, G., Ben Amar, M. & Couder, Y. Faraday instability in floating liquid lenses: the spontaneous mutual adaptation due to radiation pressure. *J. Fluid Mech.* **725**, 402–427 (2013).
37. Pototsky, A. & Bestehorn, M. Shaping liquid drops by vibration. *EPL (Europhys. Lett.)* **121**, 46001 (2018).
38. Maksymov, I. S. & Pototsky, A. Harmonic and subharmonic waves on the surface of a vibrated liquid drop. *Phys. Rev. E* **100**, 053106 (2019).
39. Bostwick, J. B. & Steen, P. H. Dynamics of sessile drops. Part 1. Inviscid theory. *J. Fluid Mech.* **760**, 5–38 (2014).
40. Chang, C.-T., Bostwick, J. B., Daniel, S. & Steen, P. H. Dynamics of sessile drops. Part 2. Experiment. *J. Fluid Mech.* **768**, 442–467 (2015).
41. Bostwick, J. B. & Steen, P. H. Dynamics of sessile drops. Part 3. Theory of forced oscillations (2016).
42. Chang, C.-T., Bostwick, J. B., Steen, P. H. & Daniel, S. Substrate constraint modifies the Rayleigh spectrum of vibrating sessile drops. *Phys. Rev. E* **88**, 023015 (2013).
43. Kumar, K. Linear theory of Faraday instability in viscous liquids. *Proc. Royal Soc. Lond. A* **452**, 1113–1126 (1996).
44. Hong, S.-H. *et al*. Wave-controlled bacterial attachment and formation of biofilms. *arXiv e-prints* arXiv:1910.13004, 1910.13004 (2019).
45. Baker, G. H., Brown, G., Butt, K., Curry, J. P. & Scullion, J. Introduced earthworms in agricultural and reclaimed land: their ecology and influences on soil properties, plant production and other soil biota. *Biol. Invasions* **8**, 1301–1316 (2006).
46. Earthworm Identification Guide for the OPAL Soil and Earthworm Survey, www.opalexplorenature.org (Accessed 20-November-2019).
47. Amabili, M. *Nonlinear Vibrations and Stability of Shells and Plates* (Cambridge University Press, 2008).

48. Kier, W. M. The diversity of hydrostatic skeletons. *J. Exp. Biol.* **215**, 1247–1257 (2012).
49. Harris, J. & Crofton, H. Structure and function in the nematodes: internal pressure and cuticular structure in *Ascaris*. *J. Exp. Biol.* **34**, 116–130 (1957).
50. McKenzie, B. M. & Dexter, A. R. Physical properties of casts of the earthworm *Aporrectodea rosea*. *Biol. Fertil. Soils* **5**, 152–157 (1987).
51. Briones, M. J. I. & Álvarez Otero, R. Body wall thickness as a potential functional trait for assigning earthworm species to ecological categories. *Pedobiologia* **67**, 26–34 (2018).
52. Simchareon, W., Amnuaikit, T., Boonme, P., Taweepreda, W. & Pichayakorn, W. Characterization of natural rubber latex film containing various enhancers. *Procedia Chem.* **4**, 308–312 (2012).
53. Backholm, M., Ryu, W. S. & Dalnoki-Veress, K. Viscoelastic properties of the nematode caenorhabditis elegans, a self-similar, shear-thinning worm. *PNAS* **110**, 4528–4533 (2013).
54. Ballesta, P. & Manneville, S. Signature of elasticity in the Faraday instability. *Phys. Rev. E* **71**, 026308 (2005).
55. Maity, D. K., Kumar, K. & Khastgir, S. P. Instability of a horizontal water half-cylinder under vertical vibration. *Exp. Fluids* **61**, 25 (2020).
56. Wang, C. Y. & Watson, L. T. The fluid-filled cylindrical membrane container. *J. Eng. Math.* **15**, 81–88 (1981).
57. Hidaka, T., Kuriyama, H. & Yamamoto, T. The mechanical properties of the longitudinal muscle in the earthworm. *J. Exp. Biol.* **50**, 431–443 (1969).
58. Tashiro, N. Mechanical properties of the longitudinal and circular muscle in the earthworm. *J. Exp. Biol.* **54**, 101–110 (1971).
59. Colbert, M.-J., Raegen, A., Fradin, C. & Dalnoki-Veress, K. Adhesion and membrane tension of single vesicles and living cells using a micropipette-based technique. *Eur. Phys. J. E* **30**, 117–121 (2009).
60. Gilpin, W., Uppaluri, S. & Brangwynne, C. P. Worms under pressure: Bulk mechanical properties of C. elegans are independent of the cuticle. *Biophys. J.* **108**, 1887–1898 (2015).
61. Nakajima, M., Ahmad, M. R., Kojima, S., Homma, M. & Fukuda, T. Local stiffness measurements of C. elegans by buckling nanoprobes inside an environmental sem. In *2009 IEEE/RSJ Int. Conf. on Intelligent Robots and Systems*, 4695–4700 (2009).
62. Arnold, R. N., Warburton, G. B. & Born, M. Flexural vibrations of the walls of thin cylindrical shells having freely supported ends. *Proc. Royal Soc. Lond. A* **197**, 238–256 (1949).
63. Warburton, G. B. Vibration of thin cylindrical shells. *J. Mech. Eng. Sci.* **7**, 399–407 (1965).
64. Lindholm, U. S., Kana, D. D. & Abramson, H. N. Breathing vibrations of a circular cylindrical shell with an internal liquid. *J. Aerospace Sci.* **29**, 1052–1059 (1962).
65. Amabili, M. Theory and experiments for large-amplitude vibrations of empty and fluid-filled circular cylindrical shells with imperfections. *J. Sound Vib.* **262**, 921–975 (2003).
66. Amabili, M. *Nonlinear Mechanics of Shells and Plates in Composite*, *Soft and Biological Materials* (Cambridge University Press, 2018).
67. Shirakawa, K. & Morita, M. Vibration and buckling of cylinders with elliptical cross section. *J. Sound Vib.* **84**, 121–131 (1982).
68. Hsu, C. On the parametric excitation of a dynamic system having multiple degrees of freedom. *J. Appl. Mech.* **30**, 367–372 (1963).
69. Maksymov, I. S. Faraday waves in earthworms: non-invasive tests of the soliton model of nerve impulses. In *Proc. 12th Australasian Workshop on Computational Neuroscience and Neural Engineering*, 12 (2019).
70. Julian, F. J. & Coldman, D. E. The effects of mechanical stimulation on some electrical properties of axons. *J. Gen. Physiol.* **46**, 297–313 (1962).
71. Berry, J. G. & Reissner, E. The effect of an internal compressible fluid column on the breathing vibrations of a thin pressurized cylindrical shell. *J. Aerosp. Sci.* **25**, 288–294 (1958).

Acknowledgements

This work was supported by the Australian Research Council (ARC) through its Future Fellowship (FT180100343).

Author contributions

I.S.M. conceived the idea and conducted the experiment. A.P. developed the theoretical model. Both authors contributed to writing and revising the manuscript and contributed to analysing and interpreting the results.

Competing interests

The authors declare no competing interests.

Additional information

Correspondence and requests for materials should be addressed to I.S.M. or A.P.

Reprints and permissions information is available at www.nature.com/reprints.

Publisher's note Springer Nature remains neutral with regard to jurisdictional claims in published maps and institutional affiliations.